Discussion

Edge detector tolerant to object defocusing

Javier Mazzaferri [a,1], Juan Campos [b], Juan C. Escalera [b], Colin J.R. Sheppard [c,d], Silvia Ledesma [a,*]

[a] Image Processing Laboratory (LPI), Physics department: 'J. J. Giambiagi', FCEyN, University of Buenos Aires, Argentina
[b] Departamento de Física, Universidad Autónoma de Barcelona, 08193 Bellatera, Spain
[c] Division of Bioengineering, National University of Singapore, 7 Engineering Drive 1, 117574, Singapore
[d] Department of Diagnostic Radiology, National University of Singapore, 5 Lower Kent Ridge Road, 119074, Singapore

ABSTRACT

Different methods for edge extraction have been studied in the past years. In a recent paper we have presented a rotation-invariant edge extractor based on a spiral phase filter placed in the frequency plane of a convergent correlator. In this architecture, the axial position of the output plane strongly depends on the axial position of the object. This condition limits the processing of three dimensional objects, because only a narrow axial region of the object would be correctly imaged to the output. The other axial regions of the target yield defocused results. Likewise, a rather small axial misalignment of planar scenes could produce completely inaccurate correlations. Besides, annular pupils have been widely used to regulate the depth of focus (DOF) and the transversal resolution of optical systems. In this paper we present a novel filter that combines the advantages of a spiral phase-based edge extractor and those of an axial-apodizing annular pupil. This design allows edge extraction of objects in a widened axial range. Numerical simulations and experimental results that demonstrate edge extraction with improved tolerance to defocusing are presented.

© 2010 Elsevier B.V. All rights reserved.

1. Introduction

Feature extraction filters have been studied both for digital and optical processings [1–8]. The interest in studying and developing optical architectures to perform image processing, has grown substantially over recent years mainly due to some real-time applications [9,10]. For instance, these kinds of devices could be implemented in combination with optical microscopes to carry out specific operations, by optical means only [11,12]. Likewise, optical processing techniques could improve in-vivo measurements, made in medical applications.

Edge extraction is a specially interesting case of feature extraction, due to its multiple applications. In some recent papers new techniques, based on a spiral phase function, have been proposed to perform image processing [13], and in particular to achieve the optical edge extraction operation, yielding very good results [11–16].

In addition, in some applications it could be of interest to perform edge extraction with three dimensional objects [17], or in planar scenes that should tolerate displacements in the axial direction. In a dynamical system, as for example a device based on optical tweezers, it should be necessary to follow the movement of particles; consequently the capability of detecting edges in different axial positions could be necessary. On the other hand, with respect to image segmentation procedures, the knowledge of edge positions makes these tasks easier to perform. In such cases, the possibility to extract edges at different axial planes could improve the segmentation of volumetric objects. It is also known that there are digital procedures to enhance defocused images; therefore these methods could be applied to complement the edge detection. However, these techniques are usually computationally intensive, and therefore the possibility to avoid digital focusing is highly convenient in real-time applications.

The proper operation of optical processing devices that are frequently employed to carry out edge extraction, depends on the precise axial positioning of the input object. This is due to the fact that the axial coordinate of the output plane, the plane where the image detector is placed, is determined by the axial coordinate of the object. This dependence on the axial position of the input prevents the processing of objects with axial depth and limits the robustness to axial misalignment in the analysis of planar scenes.

Within the fields of microscopy and lithography, some authors have addressed the design of pupils in order to tailor the 3-dimensional response of the beam [18,19], regarding both the DOF and the transversal behaviour. Perhaps the most simple and efficient of these designs are the annular phase pupils, as have been analysed in [19–21]. Regarding axial apodization, one of the stronger advantages of these pupils compared with standard circular pupils is that they could increase the DOF without reducing the numerical aperture of the optical system; i.e. without reducing the light intensity that reaches the output.

An increment of DOF is generally understood as a widening of the axial region where the focused image of a fixed object can be obtained. However, it should be noted that it also means that objects positioned within a wider axial region can be accurately imaged to the same fixed image plane. In behalf of robustness and design simplicity, optical correlation devices are often designed avoiding mechanical movements of the components. Therefore, an optical design that allows a wider axial range to place the input without moving any component, represents a meaningful improvement.

In the present work we propose a novel edge extractor filter that combines the features of an omnidirectional spiral phase-based detector with the advantages of annular pupils. This new filter is able to perform optically the omnidirectional edge extraction of either 3D objects or planar objects with increased tolerance to defocusing.

In Section 2 the design of the proposed filter is introduced, and the optical edge detection and annular apodizing pupils are described. In Section 3 we present numerical simulations employed to choose the parameters of the filter that optimize the performance of the system. The optical results that validate experimentally the proposed edge extractor are also presented in Section 3. Finally, we summarized the results of the paper in Section 4.

2. Filter design

In a previous work, we have proposed a filter to perform edge extraction with a convergent correlator architecture [14]. The rotation-invariant filter function is the 2D generalization of the 1D derivative filter $H_1 = if$, where f is the 1D spatial frequency and i is the imaginary unit. The graphs of phase and amplitude of this filter are shown in Fig. 1a–c, respectively. In order to understand how this filter performs in the 1D derivative let us consider the object function in b. As it is an odd function it can be expressed as a linear combination of sin functions. The derivative changes each sin function by a cos function multiplied by f. The phase of H_1 turns the sin functions into cos functions, while the amplitude multiplies each cos function by a factor proportional to f. The result of applying filter H_1 to this object is presented in Fig. 1d, which represents the edge extracted from the object. The graphs f, h and j in Fig. 1 show the edges extracted from object b with filters composed by the phase of H_1 and the amplitudes represented by the graphs e, g and i respectively, as described below.

If one applies the phase-only filter, composed by the phase in Fig. 1a and a constant amplitude like Fig. 1e, the edge is still enhanced,

as it is shown in Fig. 1f, but in this case, the peak is very wide, which could be unsuitable for many applications. Besides, it must be pointed out that edge extraction methods are very sensitive to noise, therefore a denoising operation is usually recommended. To this end, the filter is combined with a Gaussian low-pass filter $e^{-\left(\frac{f}{\sigma}\right)^2}$, where the parameter σ controls the cut-off frequency of the filter. The amplitude transmittance of this filter is shown in Fig. 1g and the respective edge extracted is presented in Fig. 1h. With this filter a sharp edge is obtained while the input noise is reduced.

Optical implementation of complex filters is frequently difficult to address, therefore these functions are often approximated by phase functions with binary amplitude. In Fig. 1i a binary approximation of the amplitude in Fig. 1g is presented and the edge extracted by this filter is shown in Fig. 1j. It should be mentioned that with the binary amplitude filter, ringing artifacts are appreciable around the edge peak. Anyway, a very sharp response is obtained. In the 2D generalization of this filter, the amplitude in Fig. 1i turns into the amplitude annular pupil Fig. 2a, meanwhile the step phase of Fig. 1a is reproduced in all the diametral directions with the spiral phase transmission $e^{i\theta}$, where θ is the polar coordinate in the Fourier domain. The spiral phase is shown in Fig. 2b. The 2D filter operation is analogous to the operation of the 1D version. The spiral phase filter itself performs the omnidirectional edge enhancement. Besides, the effect of the annular pupil is two-fold. On one hand, the outer radius of the ring limits the amount of noise that goes through the system. On the other hand, the presence of the inner stop produces the sharpening of the edge function, in much the same way as an annular aperture improves the resolution of an image-forming system ([22], Section 8.6). On this regard, it must be mentioned that the increment of the ratio between the inner and outer radii not only improves the resolution of the system but it also reduces the contrast due to the development of sidelobes; an undesired effect analogous to the ringing artifacts observed in the 1D case of Fig. 1j. Therefore, the choice of the ring dimensions must be a trade-off between these two effects. We have found that a ratio of 0.15 yields to a satisfactory balance [14].

As was previously mentioned in Section 1, the basic idea of the present work is to generate a novel filter that combines the advantages of a filter based on a spiral phase edge detector and those of annular apodizing pupils. Annular pupils are frequently used to increase the DOF of optical imaging systems [18], and therefore they can be used to increase the tolerance to defocusing. More generally, these pupils are
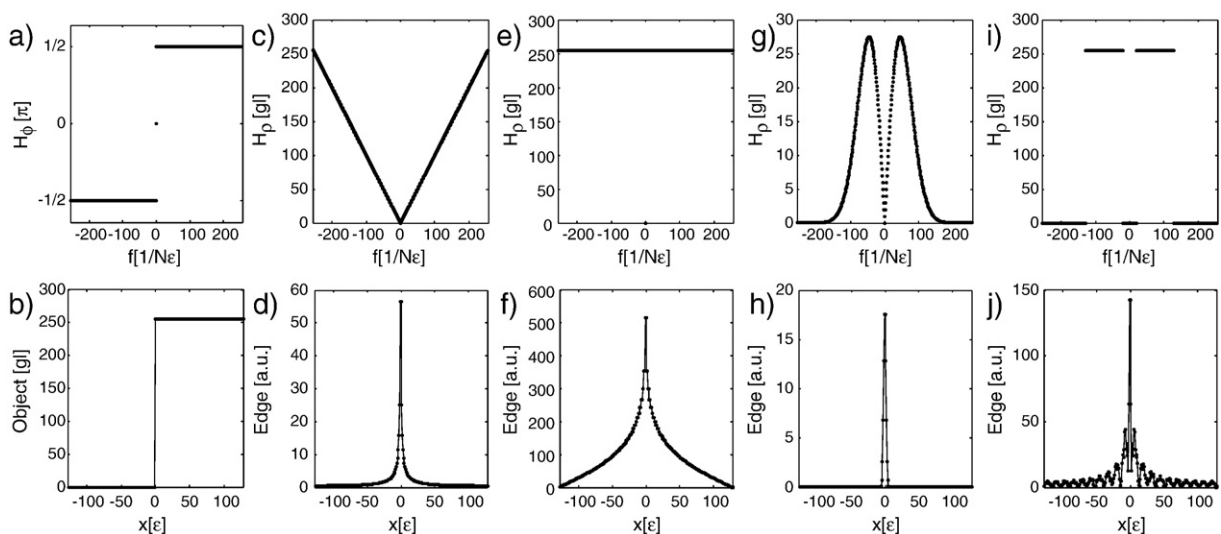

Fig. 1. Edge extraction in 1D. a) Phase of filters, b) object function, c, e, g and i) amplitudes of filters, and d, f, h, and j) edges extracted from object b with filters composed by the phase a and amplitudes c, e, g and i, respectively.
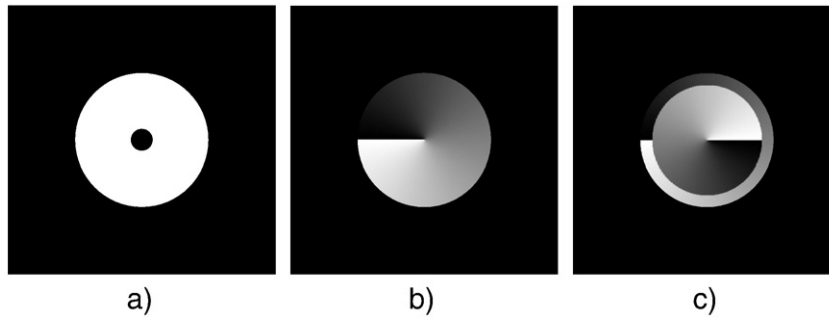
Fig. 2. a, b) Amplitude and phase of the original edge detector filter. a, c) Amplitude and phase of the edge detector filter combined with annular pupil. In a, black and white denote 0 and 1 transmissions respectively, and in b and c the gray-scale ranging from black to white denotes 0 to 2π values.

able to produce different results in an optical system depending on the parameters of the ring. Indeed, the axial and transverse responses in the best image plane (BIP) can be shaped by properly selecting these parameters [20]. All the combinations are allowed and it is possible to obtain axial and/or transverse superresolving or apodizing responses. For our method we have selected a two-zone annular filter to be combined with the edge detector, owing to its simplicity and excellent capabilities.

In general, the two-zone filters are characterized by three independent parameters; typically: the radius of the central zone normalized by the outer radius of the pupil ρ, and the modulus and phase of its transmittance [19]. As we are interested in rather specific features of the system, the parameter's space can be restricted. Indeed, if the pupil is purely real, the axial intensity is symmetrical about the BIP. Since we are concerned with maximizing the optical efficiency of the system and we are not interested in displacing the edge information from the BIP, we have chosen to employ $0-\pi$ phase-only pupils. With such constraints in the parameters, these pupils exhibit transversal responses that can be superresolving (for $p^2 < 0.5$) or apodizing (for $\rho^2 > 0.5$), while the axial response is apodizing for all possible values of ρ [19]. These facts make these annular pupils an appropriate choice for the present work. The particular value of ρ that optimizes the response of the pupil should be selected by considering the whole composed filter, as we will explain in Section 3. The whole filter, obtained as a product between the complex transmittances of the edge detector filter and the annular pupil, is shown in amplitude and phase in Fig. 2a–c, respectively.

In order to describe the behaviour of image formation systems, a non-dimensional coordinate is usually employed. This coordinate can be defined in terms of either the position of the object or the position of the image. This is due to the fact that the mentioned positions are bounded together by the Gauss's law. As it was explained in the Introduction, we are concerned with the response of the system on a fixed plane of the image space (the position of the image sensor), in terms of the variations of the position of the object. For this reason, we

define the non-dimensional coordinate u in terms of the position z_o of the object, analogously to the definition of [23], as:

$$u = kz_o \sin^2(\alpha), \tag{1}$$

where $k = 2\pi/\lambda$, λ is the wavelength of the light emitted by the source, $\sin(\alpha)$ is the numerical aperture of the system, and α is the half-angle of the maximum cone of light that can enter the imaging lens. The displacement from the best object plane (BOP) can be characterized with a relative coordinate $\Delta u = u - u_o$, where $u_o = u(z_o^0)$ and z_o^0 is the axial position of the BOP.

3. Results

3.1. Numerical simulations

It should be pointed out that the proposed edge extraction is achieved by means of a frequency filtering. Then, it is likely that the combination of the filter with an annular pupil could cause the modification of some features in the edge detection. In other words, the results obtained with the combined filter may differ from those obtained without the apodizing pupil. Therefore, the proper parameters of the pupil that compose the combined detector must be selected by considering the effect of the whole filter. In order to study the performance of the method with different apodizing pupils, we have computed numerical simulations of the edge extraction for phase rings with different values of ρ. As an input scene, we have employed the image in Fig. 3a, and the numerical simulation of a typical edge extraction is shown in Fig. 3b. Profiles as the one labelled as P in Fig. 3b, of each vertical edge were employed to evaluate the quality of edge extraction. As an example, in Fig. 3c a profile P is graphed vs. the coordinate x, orthogonal to the edge.

In Fig. 4a we show the edge height obtained for composed filters with different values of ρ, versus the defocus Δu. The full width at half maximum (FWHM) of each axial response has been computed, and
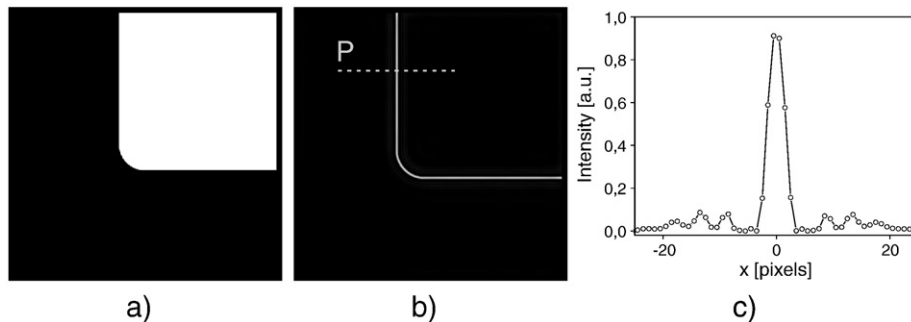

Fig. 3. a) Input scene, b) edge extracted with combined filter using pupil ring of $\rho = 0, 83$, and c) average of 100 profiles of the vertical edge in b.
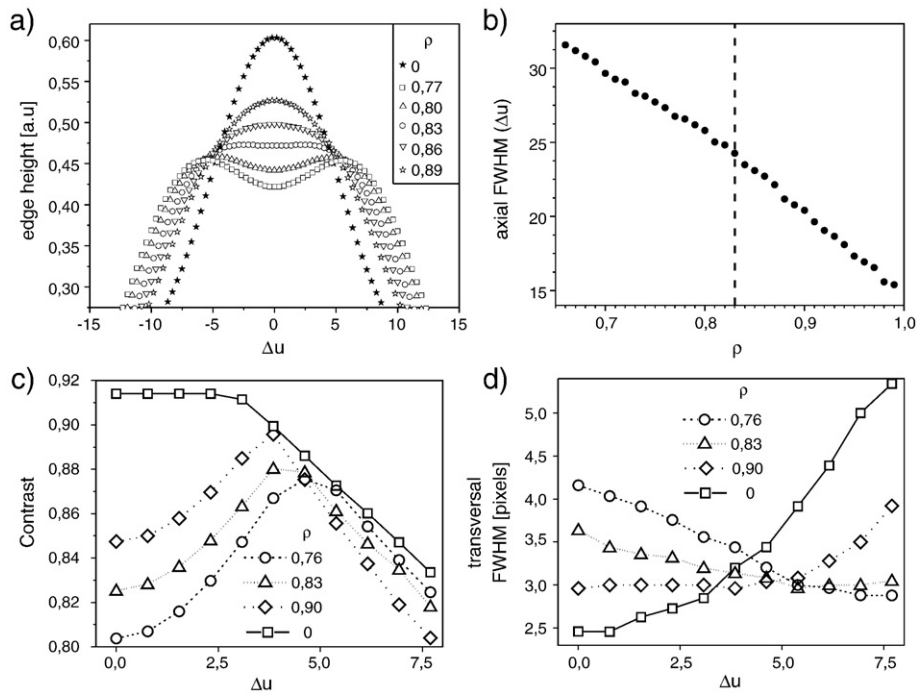
Fig. 4. Performance parameters of edge extraction obtained by numerical simulations.

graphed as a function of ρ in Fig. 4b. It must be mentioned that the composed filters present different behaviours in three disjoint ranges of ρ values. For ρ-values below 0.12 the axial response of the composed filter is hardly distinguished from that of the edge detector alone. Within the contiguous range [0.12, 0.66] an undesired distortion, consisting in a double edge, is obtained. Finally, a clear axial apodization is achieved for ρ-values higher than 0.66. For this reason, in Fig. 4, we have presented the results of numerical simulations within this last range.

As can be observed in Fig. 4b, the axial response becomes wider as ρ is reduced. In addition, if ρ takes values lower than 0.83 a minimum in the BOP appears. Therefore, $\rho = 0.83$ seems to be an appropriate value for the combined filter since it presents, simultaneously, an apodizing and almost planar axial response.

Besides, the transversal resolution and the output contrast, yielded by the new filter, are also influenced by the parameter ρ. The optimum filter should be able to extract high contrasted narrow edges from objects placed anywhere within the axial range of interest. In order to test this, we have employed two parameters that characterize the edge profiles, namely: the contrast between the peak height and the maximum side lobe, and the transversal FWHM. The parameters, for the filters with four different values of ρ, were calculated and graphed vs. Δu in Fig. 4c and d. Taking advantage of the symmetry around the BOP, which is also observable in Fig. 4a, we have graphed the mentioned parameters only for positive values of Δu. With the data presented in Fig. 4c and d we have calculated the average and the standard deviation σ of each parameter within the range [0,7.5] of Δu. This range was selected to illustrate the edge extraction inaxial coordinates where the proposed filter increases the tolerance to defocusing. The resulting values are presented in Table 1. As can be appreciated from Fig. 4 and Table 1, the pupil with $\rho = 0.83$ yields the lowest variations in the contrast and transversal FWHM. In addition, the contrast for the edge detector alone ($\rho = 0$) is reduced as the object is displaced from the BOP. When the apodizing pupils are used, the contrast is slightly lower that the obtained without pupil, but the variations in the contrast introduced by the apodizing pupils are below 3.2% of its mean value (0.85).The pupil that entails the minimum decrease of contrast is that with $\rho = 0.83$, yielding contrast

values above 0.82 in the considered range of Δu. On the basis of the analysis described above, we selected the pupil with $\rho = 0.83$ and we tested it numerically and experimentally.

The performance of edge extraction also depends on the features of the input scene. The processing of objects with small details, as well as scenes with soft edges, may present low performance. We have tested the capabilities of the proposed filter concerning these two features of the objects. On one hand, in Fig. 5 we present the numerical simulation of edge extraction of two objects with details of different sizes, processed with both, the original and the proposed filters. All the cases were studied by placing the objects either in $\Delta u = 0$ (BOP) and in $\Delta u = 7.5$. In the bottom part of the figure, the profile P for each edge has been traced. For the objects placed in the BOP, the edges obtained with both filters are sharp and clear. But when the objects are axially misaligned to $\Delta u = 7.5$, the original filter presents a wider edge, and for the object with small details, it shows a double edge. As can be noted in the figure, the proposed filter is clearly more robust to the defocusing. It presents a sharp edge, even when $\Delta u = 7.5$, and although it shows some artifacts for the object with small details, the edge can be still safely extracted.

On the other hand, we have studied the effect of the softness of the edge on the edge extraction performed by the proposed filter. It was observed that the sharpness and the contrast of the edge detection peak decrease progressively as the edges of the objects softens. In Fig. 6 we present the numerical simulation of the edge extraction

Table 1

Mean and σ for the performance parameters of the edge profile. Each value was calculated from a set of 11 values corresponding to different axial positions of the object within the range [0,7.5] of Δu. The σ values are presented as a percentage of the corresponding average value.

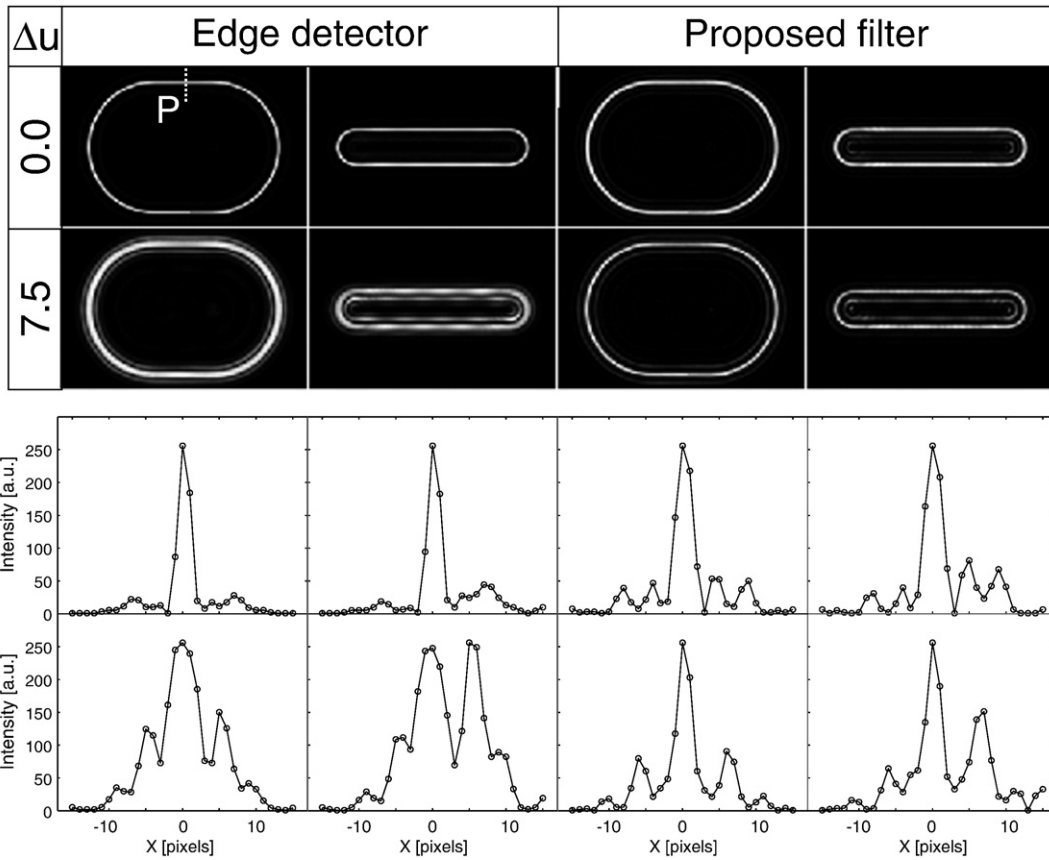| ρ	FWHM		Contrast	
	Mean	σ/mean	Mean	σ/mean
0	3.49	29.5%	0.89	3.4%
0.76	3.44	14.0%	0.84	3.0%
0.83	3.2	6.7%	0.85	2.5%
0.90	3.16	9.6%	0.85	3.2%

Fig. 5. Numerical simulations of edge extraction with the original and the combined filter of two objects with different detail sizes.

made by the proposed filter on a binary sharp object and a gray-level object with a soft edge. Also in this case, the filter was tested for objects both in $\Delta u = 0$ and $\Delta u = 7.5$. The profiles P of the detected

edges are graphed in the bottom of the figure. As it can be observed, the edge peak for the soft scene in both axial positions, is wider and has a lower contrast when compared with the sharp object in
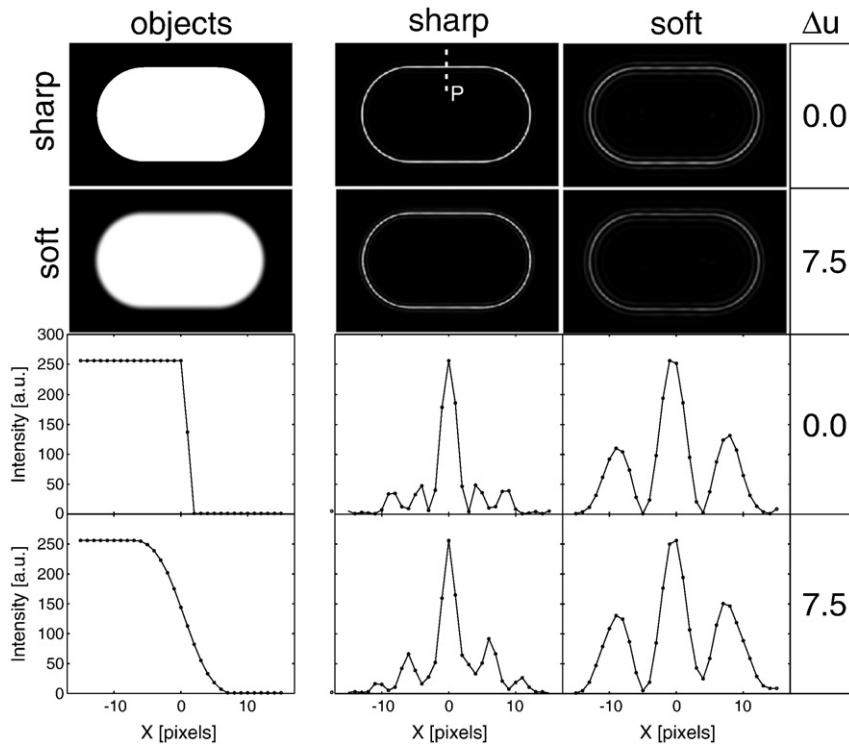

Fig. 6. Numerical simulations of edge extraction with the proposed combined filter on a sharp binary object and a soft gray-level scene.
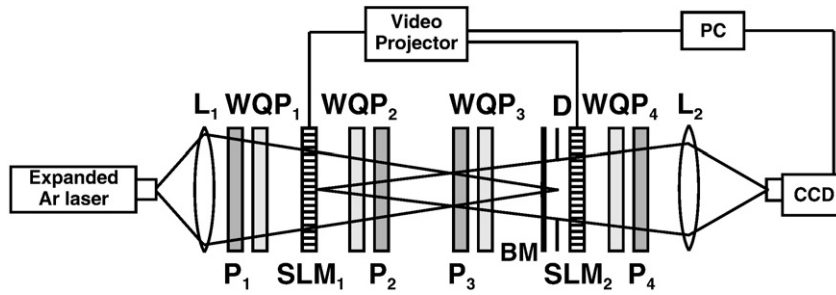
Fig. 7. Experimental set-up.

analogous situations. However, it should be noted that the filter is able to work correctly with both sharp binary and soft gray-level objects.

In the following section we present the experimental tests of the proposed method.

3.2. Experiment

The proposed edge detector was tested experimentally, and it was compared with the edge detector without apodizing pupil. The experimental set-up employed in the experiment is sketched in Fig. 7.

The expanded light from an Ar Laser ($\lambda = 457$ nm) impinges on lens L_1. The Fourier transform of the scene displayed on SLM_1 is obtained on the plane where SLM_2 is placed. Polarizers $P_1 - P_2$, and quarter-wave plates $WQP_1 - WQP_2$ configure SLM_1 to modulate the amplitude of the incident light while the phase transmission remains constant [24,25]. The amplitude of the filter is jointly represented by the binary mask BM and the diaphragm D, which are placed in contact with SLM_2, where the phase of the filter is displayed. Polarizers $P_3 - P_4$ and quarter-wave plates $WQP_3 - WQP_4$ configure SLM_2 to modulate the phase of the incident light while the amplitude transmission remains constant [24,25]. Lens L_2 images the output correlation on the CCD camera, at the end of the correlator. Both SLM_1 and SLM_2 have VGA resolution and were extracted from a video projector (Proxima Desktop Projector 5100). These displays are driven by the electronics of the video projector and a PC. The images captured by the CCD camera are acquired by the PC.

In order to test the designed filter regarding robustness to position variations we have made performance comparisons between the original edge detector and the combined filter. The input scene used for the test consists in the curved corner of binary amplitude shown in Fig. 3a. The diaphragm D was adjusted to 10.5 mm of diameter to limit the aperture of the system, hence the exit pupil is the image of D through L_2. Besides, as D limits the cone of light that reaches L_2, and

it was placed at 1.91 m from the BOP, the numerical aperture of the imaging systems was 2.75×10^{-3}.

We compared the edge images obtained with the filters of Fig. 2 for different positions of the object. We registered the edge images obtained with both filters for different z_o positions of the object, i.e. for different values of Δu.

In the left column of Fig. 8 we show the edge images for values of Δu ranging from 0 to 7.5, which in our system roughly correspond to 0 and 75 mm. It may be noted from the figure that the width of the edge increases continuously with Δu for the edge detector alone. On the contrary, with the combined filter the edge width remains almost constant.

In order to make a deeper analysis, the profiles of the edges in Fig. 8 are shown in the right column of the figure. To reduce the effects of experimental noise, we compute the average of 100 parallel traces, each of them orthogonal to the vertical edge. This procedure was carried out for each edge image.

As can be observed from the traces in Fig. 8, the response of the edge detector is degraded by the defocusing. Note the progressive increment of the edges width. Additionally, the growth of the side lobes as well as the decrement of the peak height is evident. Both aspects of the degradation are reduced significantly when the combined filter is used.

Our results demonstrate that the proposed filter, not only extracts edges optically as good as the original filter does, but it also provides a significant increase of the tolerance to defocusing.

4. Conclusions

An optical edge detector robust to defocusing was developed. The method is based on the design of a phase function which is used as a filter in a convergent optical correlator. The designed function results
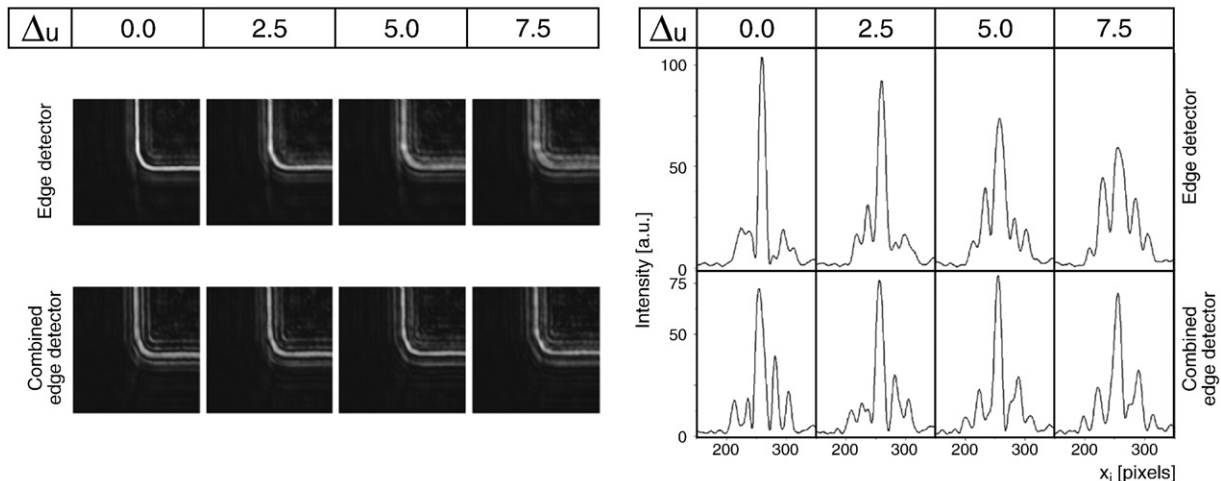

Fig. 8. Left column: experimental edge results for different values of Δu. Right column: corresponding transversal profiles of the results in the left column.

from a combination of a spiral phase, and an annular phase pupil that provides the axial apodization that reduces the effect of defocusing. The parameter ρ of the annular pupil was chosen numerically to optimize the performance of the whole edge detector. It was observed that the proposed filter presents an apodizing behaviour within the range [0.66, 1] of ρ-values. However, for values near 0.66 the axial response has a minimum at the BOP. The value of $\rho = 0.83$ yields an edge detector which exhibits axial apodization and an almost planar axial response. The filter was optically implemented in a convergent correlator, and the results demonstrate that it performs edge extraction with increased robustness to defocusing. By means of additional numerical simulations we have clarified some limitations of the method regarding the spatial resolutions of the objects and the smoothness of the edges. However, the results show that, compared to the original edge detector, the proposed method increases the tolerance to defocusing also under the aforementioned adverse conditions.

This method can be employed in optical microscopy devices to analyze edges of three dimensional objects, as well as planar objects with increased tolerance to possible defocusing.

Acknowledgement

References

[1] T. Shimada, F. Sakaida, H. Kawamura, T. Okumura, Remote Sensing of Environment 98 (2005) 21.
[2] H. Liu, K.C. Jezek, International Journal of Remote Sensing 25 (2004) 937.
[3] J. Haarpaintner, R. Tonboe, D.V. Long, M.L. Woert, IEEE Transactions on Geoscience and Remote Sensing 42 (2004) 1433.
[4] B. Tso, R.C. Olsen, Remote Sensing of Environment 97 (2005) 127.
[5] H. Tang, E. Wu, Q. Ma, D. Gallagher, G. Perera, T. Zhuang, Computerized Medical Imaging and Graphics 24 (2000) 349.
[6] A.K. Jain, H. Chen, Pattern Recognition 37 (2004) 1519.
[7] L. Yin, A. Basu, J.K. Chang, Pattern Recognition 37 (2004) 1407.
[8] P.G.V. Dokkum, Publications of the Astronomical Society of the Pacific 113 (2001) 1420.
[9] H. Zhang, C.M. Cartwright, M.S. Ding, W. Gillespie, Optics Communications 185 (2000) 277.
[10] J.E. Mazzaferri, S.A. Ledesma, C.C. Iemmi, Journal of Optics A: Pure and Applied Optics 5 (2003) 425.
[11] S. Fürhapter, A. Jesacher, S. Bernet, M. Ritsch-Marte, Optics Express 13 (2005) 689.
[12] A. Jesacher, S. Fürhapter, S. Bernet, M. Ritsch-Marte, Physical Review Letters 94 (2005) 233.
[13] K.G. Larkin, Journal of the Optical Society of America A 18 (2001) 8.
[14] J. Mazzaferri, S. Ledesma, Optics Communications 272 (2007) 367.
[15] J.A. Davis, D.E. McNamara, D.M. Cottrell, J. Campos, Optics Letters 25 (2000) 99.
[16] C.S. Guo, Y.J. Han, J.B. Xu, J. Ding, Optics Letters 31 (10) (2006) 1394.
[17] L. Fan, F. Song, S. Jutamulia, Optics Communications 270 (2007) 169.
[18] S. Ledesma, J.C. Escalera, J. Campos, M.J. Yzuel, Optics Communications 249 (2005) 183.
[19] C.J. Sheppard, J. Campos, J.C. Escalera, S. Ledesma, Optics Communications 281 (2008) 913.
[20] S. Ledesma, J.C. Escalera, J. Campos, J. Mazzaferri, M.J. Yzuel, Optics Communications 266 (2006) 6.
[21] H. Wang, Z. Chen, F. Gan, Optical Engineering 40 (6) (2001) 991.
[22] M. Born, E. Wolf, Principles of Optics 6th Edition, Pergamon Press, UK, 1983.
[23] C. Sheppard, Z.S. Hegedus, Journal of the Optical Society of America A 5 (1988) 643.
[24] A. Márquez, J. Campos, M.J. Yzuel, I. Moreno, J.A. Davis, C. Iemmi, A. Moreno, A. Robert, Optical Engineering 39 (2000) 3301.
[25] A. Márquez, C. Iemmi, I. Moreno, J.A. Davis, J. Campos, M.J. Yzuel, Optical Engineering 40 (2001) 2558.